Dynamic Au-C anchors in molecular junctions under oriented external electric fields

Rajarshi Samajdar[1,2†], Hao Yang[2,3†], Seungjoo Yi[2,3†], Chun-I Wang[4^], Michael A. Pence[2,4^], Moeen Meigooni[2,5], Seth Putnam[4], Xiaolin Liu[4], Jitong Ren[1,2], Jeffrey S. Moore[2,3,4], Emad Tajkhorshid[2,4,5,6,7], Joaquín Rodríguez-López[2,4,8], Nicholas E. Jackson[2,4], Charles M. Schroeder[1,2,3,4,5,7,8*]

[1]Department of Chemical and Biomolecular Engineering, University of Illinois Urbana-Champaign, Urbana, Illinois, 61801
[2]Beckman Institute for Advanced Science and Technology, University of Illinois Urbana-Champaign, Urbana, Illinois, 61801
[3]Department of Materials Science and Engineering, University of Illinois Urbana-Champaign, Urbana, Illinois, 61801
[4]Department of Chemistry, University of Illinois Urbana-Champaign, Urbana, Illinois, 61801
[5]Center for Biophysics and Quantitative Biology, University of Illinois Urbana-Champaign, Urbana, IL 61801
[6]Department of Biochemistry, University of Illinois at Urbana-Champaign, Urbana, Illinois, 61801, United States
[7]Department of Bioengineering, University of Illinois at Urbana-Champaign, Urbana, Illinois, 61801, United States
[8]Materials Research Laboratory, University of Illinois at Urbana-Champaign, Urbana, Illinois, 61801, United States

[†]Contributed equally, co-first author
^Contributed equally, co-second author
*Corresponding author

Abstract

Terminal anchor groups play a key role in controlling the stability and electronic properties of molecular junctions. Single molecule junctions typically consist of two terminal anchors linking organic molecules to metal electrodes. Here, we show that *p*-terphenyl derivatives containing only a single terminal anchor exhibit conductance features similar to junctions with two terminal anchors, which arises due to dynamic Au-C bond formation under oriented external electric fields (OEEFs). A set of *p*-terphenyl derivatives with one terminal anchor was prepared and characterized using automated chemical synthesis, single molecule electronics experiments, molecular dynamics (MD) simulations, and non-equilibrium Green's function-density functional theory (NEGF-DFT) calculations. Our results show that 4-amino-*p*-terphenyl (PPP) exhibits a distinct and well-defined high conductance state that is greatly diminished or absent in other *p*-terphenyl derivatives with single terminal anchors, whereas a low conductance state is observed in all amino-*p*-terphenyl derivatives due to non-covalent dimeric interactions. The electronic properties of PPP are characterized using a combination of cyclic voltammetry, electrolysis, and electron spin resonance, revealing that the high conductance state in PPP arises due to robust Au-C bond formation facilitated by a radical-based rigid resonating structure under OEEFs. A series of control experiments on junctions with different anchor groups reveals the role of primary amines in forming dynamic linkages under OEEFs. Overall, these results suggest that OEEFs can trigger Au-C bond formation leading to high conductance pathways in organic molecules containing only one terminal anchor. Insights from this work can be leveraged in the design of molecular electronic devices, particularly in understanding the mechanisms of molecular binding and junction formation.

Introduction

Molecular junctions generally consist of three main components: a molecular bridge[1] metal electrodes[2], and terminal anchor groups that electronically couple the bridge to the electrodes[3–6]. Terminal anchors[3–5] play a key role in controlling the electronic properties of single molecule junctions via molecular binding, electronic coupling, and junction stability. One class of robust terminal anchors is characterized by dative bonding interactions with metal electrodes, including amine[6,7], thiol[8], pyridine[9], and methyl thiol[10] groups. However, molecular junctions generally require two terminal anchor groups to form a closed circuit, which poses synthetic challenges that tend to restrict the chemical space in molecular junction design. From this view, new binding modalities that avoid the requirement of two terminal anchors could expand the chemical scope of the toolbox available for molecular electronics.

In addition to dative anchor groups, covalent anchors have been reported to yield stable and highly conductive molecular junctions[11]. However, direct formation of Au-C covalent bonds in molecular junctions is challenging and typically requires cleavage or reaction of functional groups such as iodine[12], alkyne[13,14], or diazonium[15,16] to generate Au-C bonds through *in situ* reactions. Recently, oriented external electric fields[17,18] (OEEFs) have gained increasing attention for their ability to reorganize the electron distribution of molecules, stabilize charge-separated resonant forms, and trigger electrochemical reactions. This strategy can be used to facilitate the formation of direct Au-C covalent linkages, without the need for cleavage of functional groups, as a new binding mechanism for single molecule electronics. Nevertheless, the structural and electronic properties that promote the formation of Au-C contacts under OEEFs is not yet fully understood.

Singly anchored molecules lack a second terminal anchor group to complete a closed electronic circuit. Prior work has reported that electron transport in singly anchored molecules occurs by non-covalent interactions such as π−π stacking[19,20] and Au-π interactions[21]. However, the unanchored terminus is exposed to strong electric fields due to the close proximity to the electrode surface in the junction, which could induce a dynamic second anchor via the formation of an Au-C bond[18]. In addition, understanding the electron transport behavior in π-conjugated molecules with one terminal anchor group could provide additional insights into non-covalent intermolecular interactions. Intermolecular charge transport[22] in π-stacked aromatic groups is critical to organic electronics[23]. The efficiency of electron transport in π-stacked systems depends on the electronic coupling and the distance and orientation between neighboring π-stacked molecules[24–26]. Although recent work has examined electron transport in singly anchored organic molecules[20,27,28], we lack a complete understanding of the potential for triggered or dynamic anchor formation for singly anchored molecules under OEEFs.

In this work, we investigate the electron transport behavior of singly anchored *p*-terphenyl derivatives using a combination of automated chemical synthesis, single molecule electronics experiments, molecular dynamics (MD) simulations, and non-equilibrium

Green's function-density functional theory (NEGF-DFT) calculations. Synthesis of *p*-terphenyl derivatives was performed using a rapid Suzuki-Miyaura cross coupling (SMCC) method with reduced reaction time and temperature[29]. Following synthesis, the electronic properties of these molecules were characterized using the scanning tunneling microscope-break junction (STM-BJ) technique[30,31]. Our results show that 4-amino-*p*-terphenyl (PPP) has a surprisingly well-defined high conductance feature despite the presence of only one terminal anchor, but this high conductance feature is greatly diminished or absent in all other terphenyl derivatives studied in this work. Our results further reveal a low conductance feature for all singly anchored amino-*p*-terphenyl derivatives studied in this work, which arises due to non-covalent intermolecular interactions. Flicker noise analysis and machine learning methods such as correlation 2D analysis and Gaussian mixture modeling (GMM) are used to understand the conductance behavior. In addition, cyclic voltammetry (CV), bulk-scale electrolysis, and electron spin resonance (ESR) were used to understand the origin of the high conductance state, which arises due to Au-C bond formation under OEEFs within the nanogap of molecular junctions[32].

Results and Discussion

Chemical synthesis and characterization

Synthesis of organic molecules for electronics experiments was carried out using Suzuki-Miyaura cross coupling (SMCC) by leveraging recent advances in iterative automated synthesis[29]. Prior SMCC conditions for automated synthesis require more than twelve hours to prepare one molecule[33]. Manual synthesis requires even longer time scales to synthesize a library of small molecules[34,35]. In this work, we used automated iterative coupling [33,36] based on a new rapid SMCC method (**Supporting Information Section S1-S3**) that significantly decreases the reaction time to ten minutes with high yield[29].

An automated small molecule synthesizer (**Figure 1a)** capable of parallel runs of deprotections, couplings, and purifications was used, as previously reported[33]. The building blocks and protecting groups used in the reaction are shown in **Figure 1b**. The synthesis of 4''-methyl-[1,1':4',1''-terphenyl]-4-amine (MPP), 3-fluoro-[1,1':4',1''-terphenyl]-4-amine (PPF), N-methyl-[1,1':4',1''-terphenyl]-4-amine (PPS), and 4-([1,1'-biphenyl]-4-yl) pyridine (PPN) was carried out using one step slow release SMCC chemistry (**Figure 1c**). 2'-methyl-[1,1':4',1''-terphenyl]-4-amine (PMP) and 3-methyl-[1,1':4',1''-terphenyl]-4-amine (PPM) were synthesized using a two-step synthesis process: rapid SMCC followed by slow release SMCC (**Figure 1d**). Synthesized molecules were characterized using mass spectrometry and ^{1}H and ^{13}C nuclear magnetic resonance (NMR) spectrometry (**Supplementary Figures 1-12**). [1,1':4',1''-terphenyl]-4-amine (PPP) and 1,1',4',1''-terphenyl-4-thiol (PPT) were purchased from Sigma Aldrich.

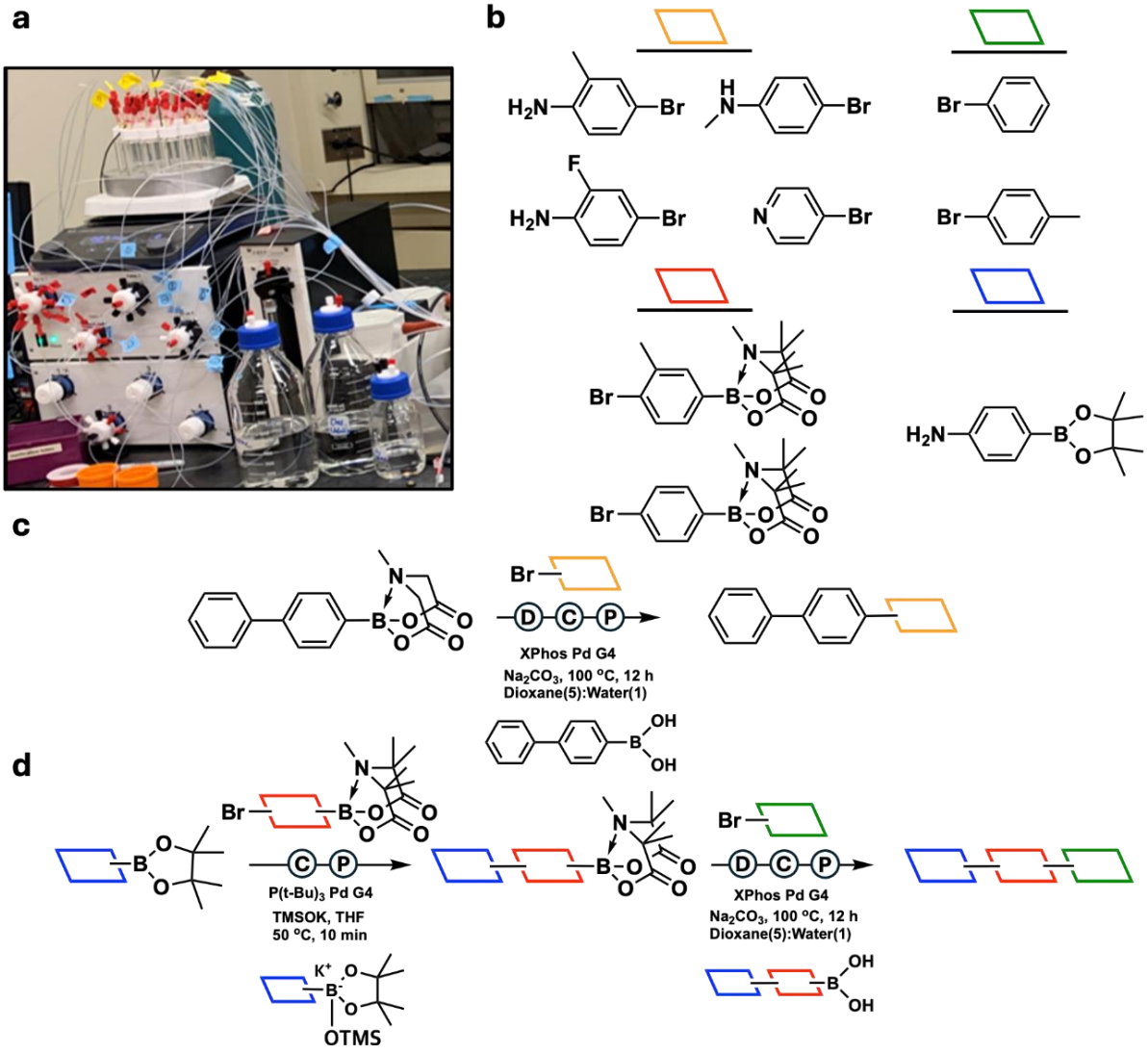

Figure 1: Overview of automated chemical synthesis method. (a) Picture of automated synthesis instrument in our lab for organic molecule synthesis based on Suzuki-Miyaura cross coupling (SMCC). (b) Summary of molecular building blocks and boronate protecting groups. (c) One-step slow release SMCC synthesis. (d) Two-step synthesis, consisting of rapid SMCC followed by slow release SMCC.

In this work, the chemical space (**Figure 2a**) focuses on *p*-terphenyl molecules for molecular electronics due to their rigidity and extended π-conjugation, which results in low tunneling barriers[37–40]. We designed a series of singly anchored *p*-terphenyl molecules based on the parent molecule PPP by including additional substituents on the three benzene rings. PPM, PMP, and MPP each contain a methyl group on one of the aromatic rings, which changes preferred resonance structures, alters ring torsional

angles, or introduces steric hindrance during the formation of molecular junctions. Molecule PPF was incorporated to investigate the effect of electron withdrawing groups in contrast to the electron donating nature of the methyl substituted terphenyls. Three additional control molecules, PPN, PPS, and PPT, are characterized to understand the role of chemical anchor groups.

Single molecule conductance measurements

The electronic properties of *p*-terphenyl derivatives were characterized at the single molecule level using the scanning tunneling microscope-break junction (STM-BJ) technique[30,31]. The STM-BJ setup consists of a gold tip electrode that is repeatedly moved into and out of contact with a gold substrate electrode in a solution containing molecules, resulting in the continual formation and breakage of single molecule junctions (**Supporting Information Section S1**). The STM-BJ instrument is automated, and experiments are repeated over an ensemble of >5000 molecules for each experiment. Single molecule conductance data are then analyzed using one- and two-dimensional (1D and 2D) conductance histograms without data selection. The timescale of a single STM-BJ pulling trajectory is in the order of milliseconds[41], which allows for sampling a range of molecular conformations[42] during a conductance measurement. Prior to understanding the electron transport behavior of singly anchored terphenyl derivatives, we characterized the molecular conductance behavior of the molecular analog with two terminal anchor groups (4,4'-diamino-*p*-terphenyl), and our results reveal a bimodal conductance distribution, with a prominent high conductance feature and weak low conductance feature, consistent with prior literature[6] (**Supplementary Figure 13**).

Single molecule conductance traces for PPP unexpectedly show two distinct populations, as demonstrated by characteristic single molecule conductance traces for high and low conductance features (**Figure 2b**). Singly anchored molecules are generally thought to form active junctions through intermolecular stacking interactions[19,20], where two different molecules, each anchored to a different electrode, form non-covalent dimeric interactions to complete the circuit. We hypothesized that the low-conductance feature in singly anchored *p*-terphenyl derivatives arises due to intermolecular stacked junctions (**Figure 2c**). However, in the STM-BJ setup, the applied bias between the two electrodes results in relatively high electric field gradients in the nanoscale junction, thereby giving rise to an OEEF[17,18]. We posited that OEEFs can induce a dynamic anchor in molecular junctions involving the formation of a new second anchor (**Figure 2d**) without requiring the cleavage or chemical reaction of additional functional groups. We aimed to understand if OEEFs could give rise to dynamic covalent anchors resulting in well-defined[43] conductance pathways in singly anchored organic molecules.

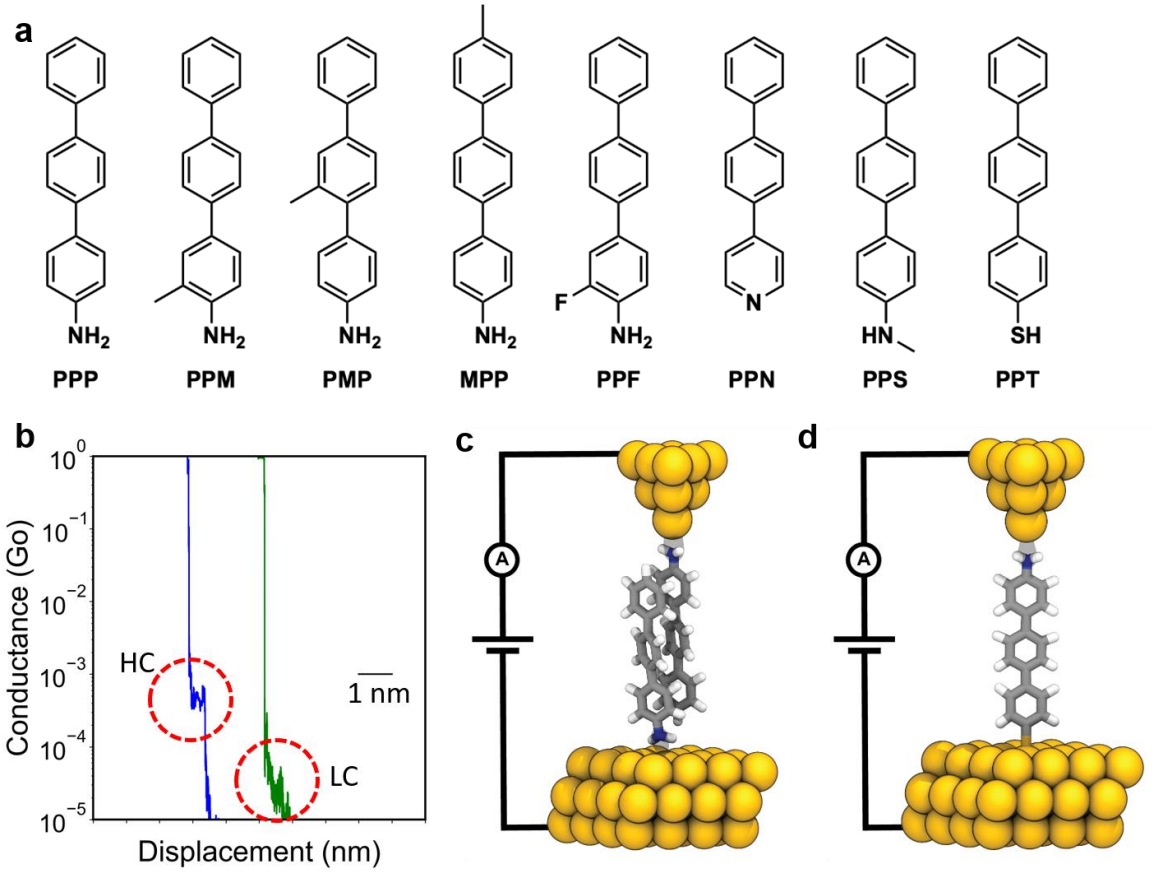

Figure 2: Molecular library and electron transport mechanisms for singly anchored terphenyl derivatives. (a) Structures of singly anchored organic molecules studied in this work. (b) Characteristic single molecule conductance traces observed in STM-BJ experiments for PPP. HC denotes the high conductance state, whereas LC denotes the low conductance state. (c) Molecular junction schematic with non-covalent dimeric interactions for PPP. (d) Molecular junction schematic featuring an Au-C bond for PPP.

We began by characterizing the electron transport properties of amino-*p*-terphenyl derivatives in non-polar solvents (1,2,4-trichlorobenzene, TCB) using the STM-BJ method. Our results show that amino-*p*-terphenyl derivatives exhibit a characteristic low conductance feature (**Figure 3a** and **Supplementary Figure 14**). Surprisingly, PPP shows an additional high conductance feature occurring in a significant molecular sub-population over a large ensemble of molecules (**Figure 3b**). Unsupervised machine learning (**Supporting Information Section S1**), 2D correlation analysis, and Gaussian mixture modeling (GMM), were used to interpret the two-state conductance behavior observed for PPP. 2D correlation analysis and GMM indicates that the two conductance

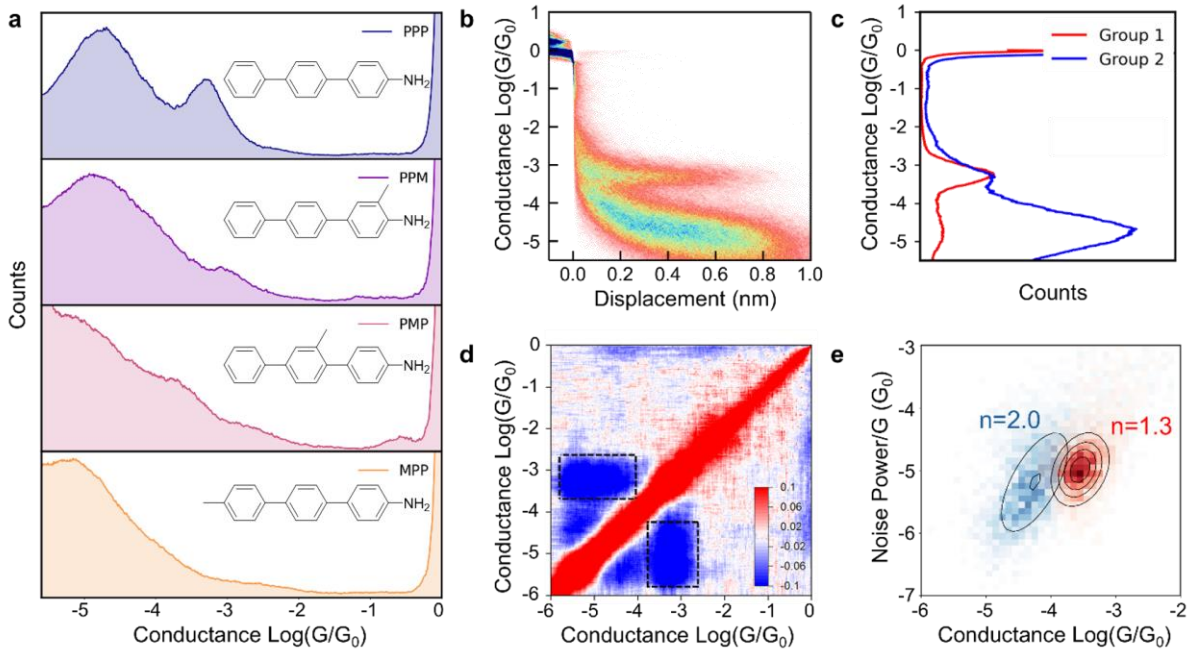

Figure 3: Scanning tunneling microscope-break junction (STM-BJ) measurements of amino-*p*-terphenyl derivatives in 1,2,4-trichlorobenzene (TCB) at 250 mV applied bias. (a) 1D conductance histograms for PPP, PPM, PMP, and MPP. (b) 2D conductance histogram for PPP. (c), (d) Gaussian mixture modeling and 2D correlation analysis on PPP revealing anti-correlated high and low conductance states. (e) Flicker noise analysis of molecular sub-populations corresponding to the high and low conductance feature for PPP, which suggests through-bond and through-space characteristics for the high and low conductance features (scaling exponents of $n \approx 1.3$ and $n \approx 2$, respectively).

states are negatively correlated and therefore occur independently in distinct trajectories during the STM-BJ experiments (**Figures 3c, d**). These results suggest that the two conductance populations arise from two different junction configurations.

Flicker noise analysis[44] was performed to differentiate between through-bond and through-space electron transport for the high and the low conductance states (**Supporting Information Section S1**). Prior work has shown that the conductance fluctuations (conductance noise power) exhibit a power law dependence on the mean conductance G values depending on through-space and through-bond transport characteristics[6,45]. Conductance noise is quantified by numerically integrating the conductance noise power spectral density (PSD) between frequencies of 100 and 1000 Hz[22,46]. The correlation is quantified by the scaling exponent n of the normalized noise power (noise power/G^n) versus the average normalized conductance G/G_0, where G_0 is the conductance quantum. A scaling exponent $n \approx 2$ suggests through-space transmission whereas an exponent $n \approx 1$ corresponds to through-bond transport. These results show

that the low conductance state in PPP occurs by through-space electron transport, whereas the high conductance state shows dominant through-bond electron transport characteristics (**Figure 3e**). Flicker noise analysis for MPP (**Supplementary Figure 15**) is also consistent with through-space electron transport for the low conductance state. Based on these results, we posit that the low conductance state observed for all amino-*p*-terphenyl derivatives in this work arises due to non-covalent dimeric interactions. We posit that the high conductance state in PPP arises due to the formation of a dynamic covalent anchor binding to the metal electrode, which is consistent with through-bond transport for the high conductance state. Based on the structure of PPP, we hypothesize that the second anchor involves the formation of an Au-C bond under the influence of OEEFs. To explore this hypothesis further, we pursued a series of additional experiments and simulations.

2D conductance histograms for amino-*p*-terphenyl derivatives indicate stark differences in electron transport pathways for different molecular composition. Notably, the high conductance state observed in PPP is significantly diminished or absent in all other singly anchored *p*-terphenyl molecules studied in this work (**Figure 3a** and **Supplementary Figure 14**), suggesting that molecular substituents disrupt the high conductance pathway in PPP. Although PPM and PMP show a weak high conductance feature, it is completely absent in MPP, implying that the presence of a methyl group at the para position on the aromatic ring completely abolishes the high conductance pathway. OEEFs are known to stabilize charge resonance structures and catalyze chemical reactions[17,18]. It is possible that the quinoidal resonant form of the axisymmetric molecule PPP is relevant for electron transport, with electron density redistributing towards the para position on the phenyl ring farthest from the amine anchor.

We hypothesize that the carbon atom at the terminal para position in amino-*p*-terphenyl derivatives PPP, PPM, and PMP forms a direct Au-C covalent linkage, creating a single molecule bridge that completes the circuit and leads to the high conductance pathway (**Figure 2d**). The absence of the high conductance feature in MPP is consistent with the hypothesis that the methyl group at the terminal para position inhibits the interaction between the molecule and the gold electrode, preventing the formation of the Au-C covalent linkage. However, the para position remains available for binding in PPM and PMP, but the substituent groups on these molecules disrupt their symmetry, which disfavors the formation of the quinoidal resonant form. PMP contains a methyl substituent on the central ring, which alters the torsional angles and hinders the formation of the planar quinoidal resonant form, resulting in a weak high conductance feature compared to PPP.

We further characterized the electronic properties of PPF, which contains an electron withdrawing group as opposed to the electron donating group in the methyl substituted terphenyl molecules. PPF exhibits similar electron transport characteristics to PPM (**Supplementary Figure 16**), suggesting that the nature of substituent does not

significantly affect the high conductance state. These results indicate that disruption of symmetry in the amino-*p*-terphenyl derivatives can inhibit the high conductance state. In addition, we also characterized the electronic properties of PPN, PPT, and PPS, which contain thiol, pyridine, and N-methylamino as terminal anchor groups, respectively. The electron transport behavior of PPN, PPT, and PPS (**Supplementary Figure 17**) indicates the absence of a high conductance state in these molecules. PPN exhibits a low conductance state, which is absent or significantly diminished in PPT and PPS, and likely arises due to non-covalent dimeric interactions.

We conducted a series of additional single molecule experiments by varying temperature, concentration, and applied bias to further understand the high- and low-conductance populations observed for PPP. Temperature-dependent STM-BJ measurements were carried out at three different temperatures: 20 ^{0}C, 30 ^{0}C and 40 ^{0}C. Increased temperature leads to enhanced molecular vibrations, reducing the likelihood of forming intermolecular junctions during the STM-BJ experiments[47]. Our results indicate that as the temperature is increased, the low conductance state is significantly diminished (**Figure 4a**). These results are consistent with our hypothesis that the low conductance state arises due to non-covalent dimeric interactions. On the other hand, the high conductance state is largely unaffected by the 20ºC temperature increase, suggesting the high conductance state arises due to a stronger binding mechanism. Concentration-dependent STM-BJ experiments were also performed for PPP in the range on 0.1-10 mM (**Figure 4b**). These results indicate that the low conductance state of PPP exhibits strong concentration dependence, whereas the high conductance state is concentration independent. These results are consistent with our hypothesis that the low conductance state arises due to non-covalent dimeric interactions whereas the high conductance state arises due to through-bond transport.

Bias dependent STM-BJ experiments (**Figure 4c**) reveal that at low applied bias (50-150 mV), only the high conductance state is observed. These results indicate that even at relatively low applied biases, OEEFs are sufficient to induce Au-C linkages. As the applied bias is increased, the low conductance state emerges, consistent with prior work reporting that increased bias regulates dimeric interactions in molecular junctions[28]. The two-state conductance characteristic of PPP is also observed in a polar solvent such as propylene carbonate (PC), but with lower counts for each conductance population as the higher dielectric strength of polar solvents likely reduces the effect of OEEFs[18] (**Figure 4d**). We also characterized the molecular conductance of PPP in PC in the presence of a reducing agent (sodium borohydride, $NaBH_4$), which results in the disappearance of the high conductance state (**Supplementary Figure 18)**. Based on these results, we posit that a charge separated quinoidal resonant form of PPP is involved for the high conductance state. Overall, results from STM-BJ experiments indicate that the high conductance in PPP state involves monomeric through-bond electron transport.

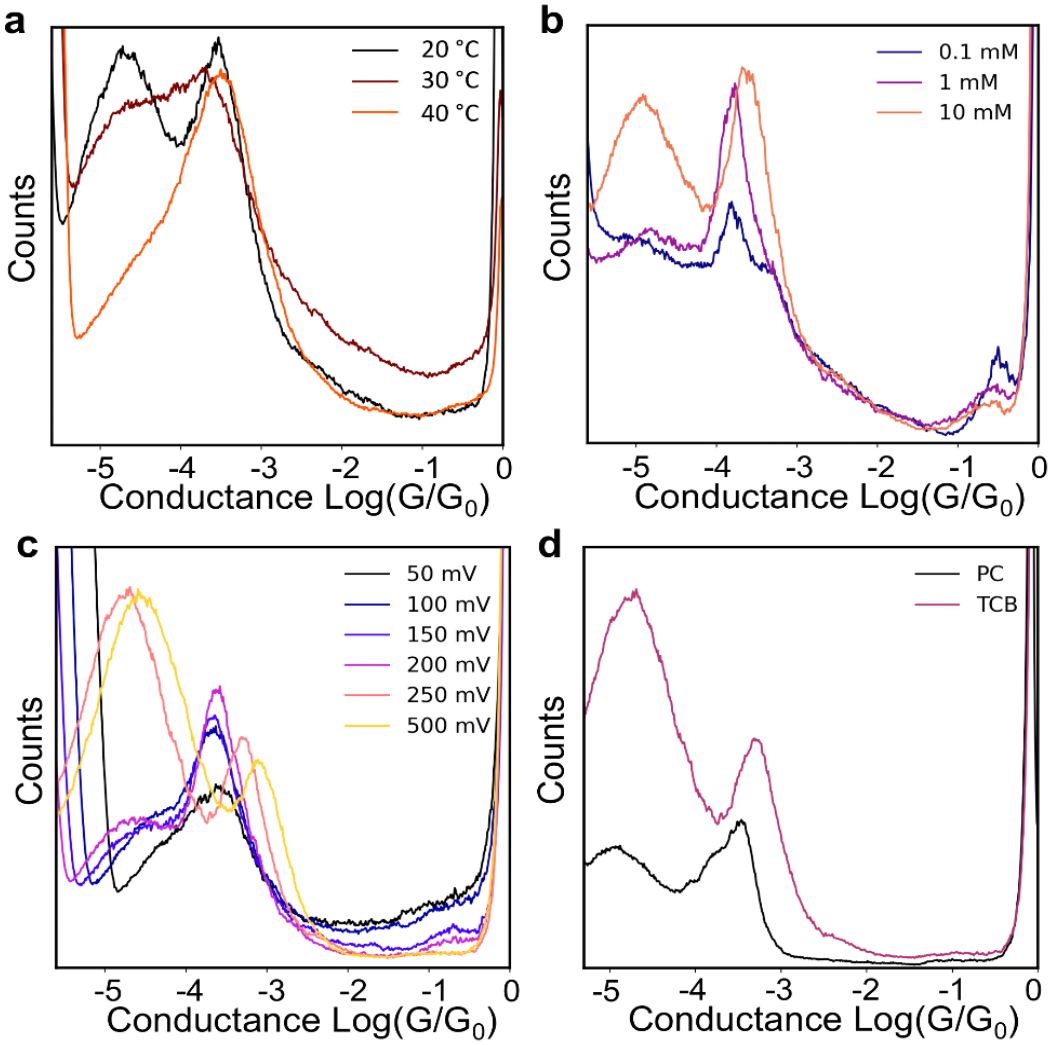

Figure 4: Effect of temperature, concentration, and applied bias on the molecular conductance of PPP. (a) Temperature-dependent conductance measurements are consistent with non-covalent dimeric interactions for low conductance state, whereas the high conductance state is robust to temperature variations. (b) Concentration-dependent measurements for PPP. (c) Bias-dependent STM-BJ experiments indicating that the high conductance state is observed at low bias, whereas the high conductance state has bias dependence. (d) Solvent dependent STM-BJ measurements indicating that the bimodal conductance distribution is observed in non-polar (1,2,4-trichlorobenzene, TCB) and polar (propylene carbonate, PC) solvents.

Bulk electrochemistry and spectroscopy

Integrating single molecule measurements with bulk experiments offers a powerful approach to understand electron transport[48,49]. We performed a series of bulk electrochemical and spectroscopy experiments to understand the electronic properties of PPP, focusing on the origin of the high conductance state. Results from cyclic voltammetry (CV) experiments show a distinct oxidation wave on the forward scan at approximately 0.65 V vs. Ag/AgCl, with only a small reduction peak at 0.15 V on the return scan (**Figure 5a**). The absence of a prominent return peak in the CV indicates that a distinct chemical process occurs after oxidative electron transfer. A second distinct electron transfer event was observed when the positive limit of the potential window was expanded from 0.8 V to 1.0 V, however this second electron transfer event leads to the formation of a surface-bound species (**Supplementary Figure 19**). Bulk electrolysis was performed to identify the nature of the products generated upon electrochemical oxidation of PPP. The potential was maintained at 0.8 V during electrolysis to isolate the first electron transfer event and avoid possible film formation on the electrode surface. The solution in the working electrode compartment exhibited dramatic changes in color, changing from colorless to purple upon oxidation (**Figure 5b**). All electrochemical experiments were performed in triplicates, and the integrated charge was used to determine the total number of electrons transferred during the electrochemical oxidation. Our results (**Figure 5c**) indicate that one electron was transferred, which suggests that the electrochemical oxidation of PPP forms a radical cation species.

Electron spin resonance (ESR) spectroscopy experiments were performed on PPP before electrolysis, after electrolysis, and after preconcentration of the electrolysis product, as shown in **Figure 5d.** The signals at ~3480 G and ~3650 G indicate the presence of a radical species in the electrolyzed solutions that is not present in the pre-electrolyzed sample. Based on these results, we posit that the high conductance state of PPP arises due to a radical species (**Supplementary Figure 20**), which leads to the formation of a dynamic anchor based on a covalent Au-C linkage (**Figure 2d**). Computational modeling including MD simulations and NEGF-DFT calculations was further pursued to complement experimental results.

Molecular dynamics (MD) simulations

MD simulations have been used to characterize complex molecular geometries or conformations adapted by molecular junctions[42], enabling comparison between experimental and theoretical results. Here, we used MD simulations to characterize the non-covalent dimeric interactions that resemble the low conductance state observed in the single molecule experiments.

A series of MD simulations was performed to elucidate the dimeric interactions between methyl substituted amino-*p*-terphenyl derivatives. For each terphenyl derivative, a pair of molecules was simulated in TCB and PC solvents, and the separation distance between

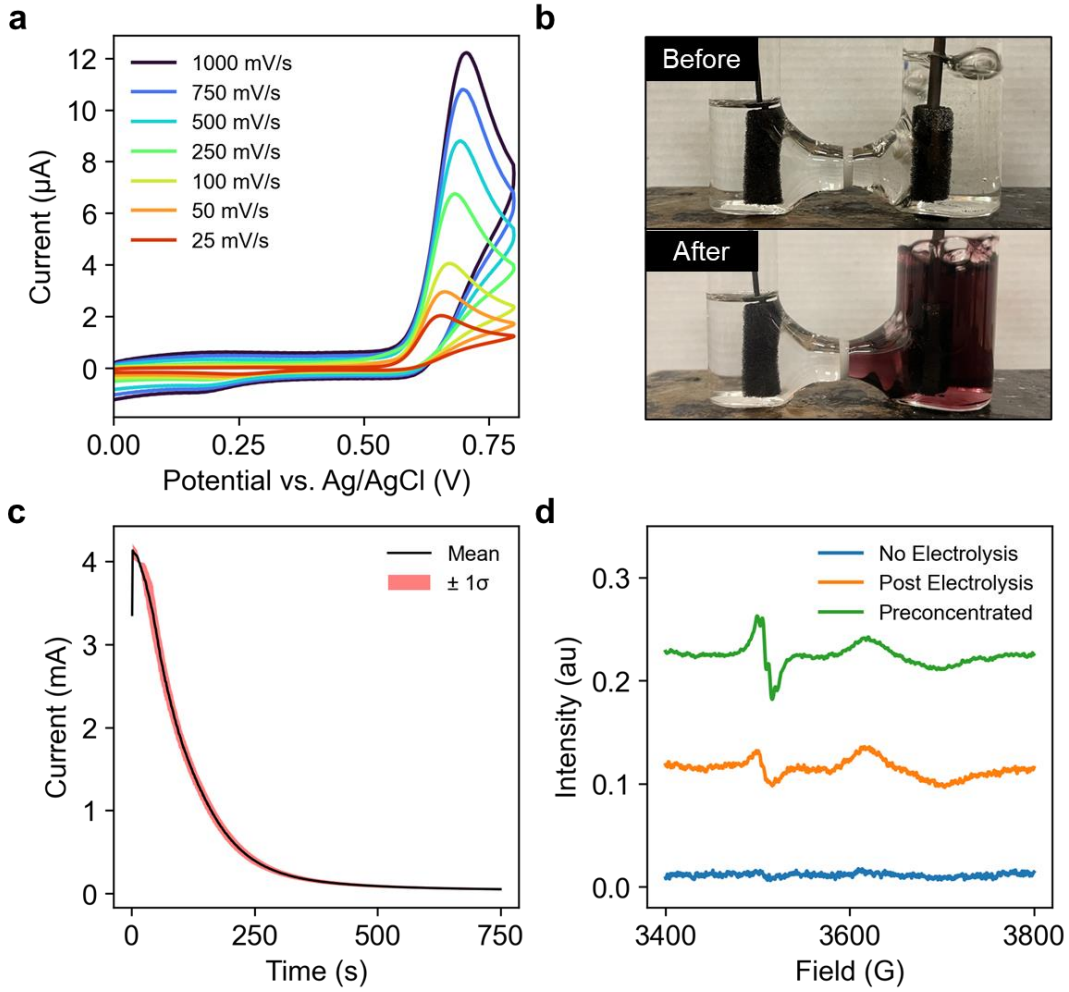

Figure 5. Bulk electrochemistry and spectroscopy experiments on PPP. **(a)** Cyclic voltammetry of 1 mM PPP in an electrolyte solution of 0.1 M $TBAPF_6$ in PC. The potential was swept from 0 V vs. Ag/AgCl to 0.8 V vs. Ag/AgCl in forward and reverse scans at rates ranging from 25 mV/s up to 1 V/s. **(b)** Images of a bulk electrolysis cell before and after electrolysis, showing the dramatic color change in the working electrode compartment (right) upon oxidation. **(c)** Bulk electrolysis of 1 mM PPP in an electrolyte solution of 0.1 M TBAPF6 in PC, at an applied potential of 0.8 V, taken in triplicate (N = 3). The black trace indicates the mean, and the red error bar represents 1 standard deviation from the mean. The average number of electrons transferred was 1.1 ± 0.1. **(d)** ESR spectra of the 1 mM PPP with no electrolysis, directly after electrolysis, and after electrolysis with a preconcentration step.

their center-of-mass (COM) positions was systematically varied to provide molecular insights from both energetic and conformational perspectives (**Supporting Information Section S1**). The potential mean force (PMF) as a function of the separation distance between the COM of terphenyl pairs in solution was assessed using umbrella sampling and the Weighted Histogram Analysis Method (WHAM)[50].

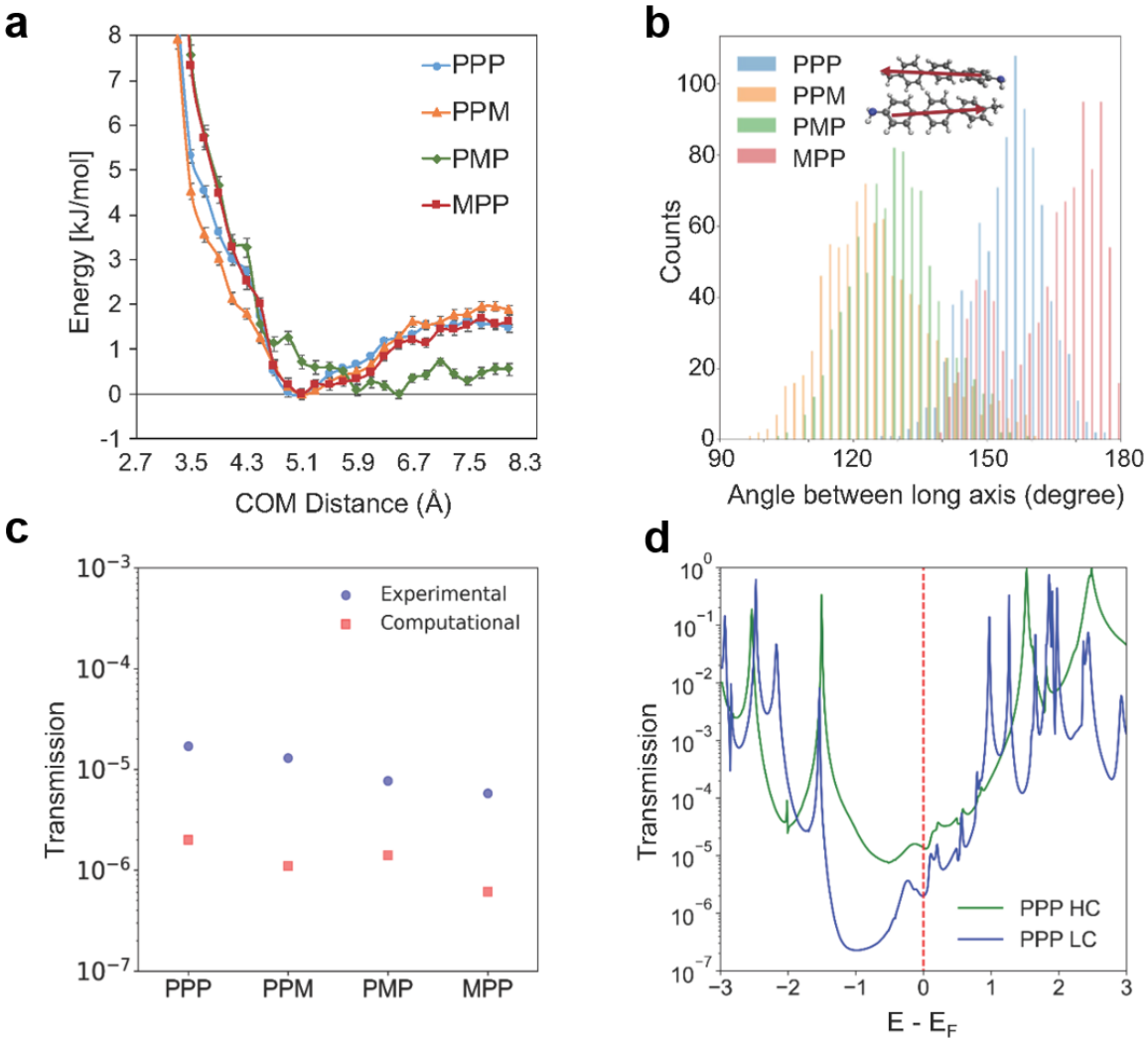

Figure 6. Molecular dynamics (MD) simulations and non-equilibrium Green's function-density functional theory (NEGF-DFT) calculations. **(a)** Potential mean force (PMF) profiles for dimers. **(b)** Distribution of the angle between the long axes of terphenyl molecules in 1,2,4-tricholorobenzene (TCB). Arrows in the inset represent the long-axis vector. **(c)** Experimental and computational transmission values at the Fermi energy level for the stacked molecular conformations for several amino-*p*-terphenyl derivatives. **(d)** Transmission plots for the high and low conductance state of PPP.

The PMFs of PPP, MPP, and PPM in TCB solution exhibit similar profiles, with the global minima located at a separation distance of 5.1 Å (**Figure 6a**). The corresponding binding energies (**Supplementary Table 1**) between two terphenyl molecules is 0.63 ± 0.04 k_BT for PPP, 0.68 ± 0.05 k_BT for MPP, and 0.79 ± 0.04 k_BT for PPM, where T is the absolute temperature at 300 K. On the other hand, the global minimum of PMP is situated at a separation distance of 5.9 Å with a binding energy of 0.19 ± 0.05 k_BT due to the non-

planar intramolecular conformation and steric hinderance caused by its methyl group at the middle phenyl ring (**Supplementary Figure 21**). The observed binding energies for the terphenyl derivatives are below 1 k_BT, which is consistent with results from the temperature-dependent STM-BJ experiments.

We further characterized the structural features of the terphenyl molecules based on the MD trajectories of the PMF global minimum. **Figure 6b** shows the angle distribution between the long axes of terphenyl molecules in TCB solvent, which quantifies the intermolecular structure between terphenyl dimers. An angle close to 180^0 indicates that the terphenyl molecules are aligned in the same parallel direction, increasing the likelihood of π-π stacking and providing an efficient conductance pathway. For MPP, a bimodal distribution is observed which could arise due to the methyl group leading to an offset in stacking for the dimeric structure. The symmetric geometry of PPP in TCB promotes a more parallel pair structure, ensuring an effective stacked dimeric structure. A similar trend in PMFs and conformational features was observed for peptides in PC solution (**Supplementary Figure 22**). Molecular conformations generated by MD can be used in computationally efficient quantum mechanics (QM) calculations to aid in comparison between theory and experimental results.

Electron transport calculations

Electron transport calculations provide a powerful tool to validate experimentally observed conductance behavior[42,43]. NEGF-DFT simulations were performed for methyl substituted amino-*p*-terphenyl derivatives in a stacked dimer geometry, corresponding to the low conductance state characterized by non-covalent intermolecular interactions (**Supporting Information Section S1**). For PPP, NEGF-DFT calculations were further carried out for the proposed high conductance state involving Au-C covalent linkages. Transmission plots for the stacked dimeric structures for PPP, PPM, and PMP show qualitatively similar behavior (**Supplementary Figure 23**). Comparing the transmission values at the Fermi energy level (**Figure 6c**) shows that MPP exhibits lower conductance compared to the other derivatives, in both experiments and NEGF-DFT calculations. These results suggest that the presence of a methyl group at the terminal para position on the phenyl ring opposite to the amine can cause an offset in stacked molecular conformation. These results also support experimental results suggesting that the low conductance state arises due to non-covalent dimeric interactions.

We also performed NEGF-DFT calculations for the high conductance state of PPP, which involves the formation of an Au-C covalent bond. Our results indicate that there is a tenfold difference in computed transmission values between the high and low conductance states of PPP (**Figure 6d**), in accordance with our experimentally observed STM-BJ results. The differences between experimental and computed transmission values could arise due to the semi-local exchange-correlation functional (PBE) used in our calculations, which tends to underestimate the HOMO-LUMO gap between the electrodes and molecule. In addition, the electron transmission calculations are carried out at zero applied bias. The

experimental STM-BJ results indicate an increase in conductance with an increase in bias. Overall, NEGF-DFT calculations combined with MD simulations support the hypothesis that the low conductance state arises due to non-covalent intermolecular interactions and the high conductance state involves the formation of a robust Au-C covalent linkage.

Conclusions

In this work, the electronic properties of singly anchored amino-*p*-terphenyl derivatives are characterized using automated chemical synthesis, single molecule electronics experiments, bulk scale electrochemistry, MD simulations, and NEGF-DFT calculations. Single molecule experiments reveal two well-defined conductance pathways in some amino-*p*-terphenyl derivatives due to the formation of robust Au-C covalent linkages under OEEFs. Bulk electrochemistry and spectroscopy experiments show that a radical cation state occurs when PPP is exposed to an electric field, which facilitates the formation of robust Au-C covalent linkages. Our results show that the formation of Au-C linkages is favored when the charge separated resonant state experiences minimal disruption. The introduction of substituents on the three benzene rings within the terphenyl system disrupts this state, hindering the high-conductance electron transport pathway. In addition, our work highlights the importance of non-covalent dimeric interactions in molecular electronics that can be leveraged for the design of materials for bulk scale measurements. MD simulations are used to understand the stacking conformations for various amino-*p*-terphenyl derivatives, and NEGF-DFT calculations are carried out to understand the electron transport behavior observed in single molecule experiments. Overall, our work highlights the role of OEEFs in generating dynamic anchor groups in molecular junctions without requiring the cleavage or conversion of functional groups, which enhances the chemical toolbox available for constructing molecular electronics.

References

1. Chen, Hongliang, and J. Fraser Stoddart. "From molecular to supramolecular electronics." *Nature Reviews Materials* **6**, 804-828 (2021).
2. Li, Songsong, Hao Yu, Xinyi Chen, Andrew A. Gewirth, Jeffrey S. Moore, and Charles M. Schroeder. "Covalent Ag–C bonding contacts from unprotected terminal acetylenes for molecular junctions." *Nano letters* **20**, 5490-5495 (2020).
3. Hong, Wenjing, David Zsolt Manrique, Pavel Moreno-García, Murat Gulcur, Artem Mishchenko, Colin J. Lambert, Martin R. Bryce, and Thomas Wandlowski. "Single molecular conductance of tolanes: experimental and theoretical study on the junction evolution dependent on the anchoring group." *Journal of the American Chemical Society* **134**, 2292-2304 (2012).
4. Kaliginedi, Veerabhadrarao, Alexander V. Rudnev, Pavel Moreno-García, Masoud Baghernejad, Cancan Huang, Wenjing Hong, and Thomas Wandlowski. "Promising anchoring groups for single-molecule conductance measurements." *Physical Chemistry Chemical Physics* **16**, 23529-23539 (2014).
5. Ward, Jonathan S., Andrea Vezzoli, Charlie Wells, Steven Bailey, Samuel P. Jarvis, Colin J. Lambert, Craig Robertson, Richard J. Nichols, and Simon J. Higgins. "A Systematic Study of Methyl Carbodithioate Esters as Effective Gold Contact Groups for Single-Molecule Electronics." *Angewandte Chemie* **136**, e202403577 (2024).
6. Magyarkuti, András, Olgun Adak, Andras Halbritter, and Latha Venkataraman. "Electronic and mechanical characteristics of stacked dimer molecular junctions." *Nanoscale* **10**, 3362-3368 (2018).
7. Quek, Su Ying, Maria Kamenetska, Michael L. Steigerwald, Hyoung Joon Choi, Steven G. Louie, Mark S. Hybertsen, J. B. Neaton, and Latha Venkataraman. "Mechanically controlled binary conductance switching of a single-molecule junction." *Nature nanotechnology* **4**, 230-234 (2009).
8. Inkpen, Michael S., Zhen–Fei Liu, Haixing Li, Luis M. Campos, Jeffrey B. Neaton, and Latha Venkataraman. "Non-chemisorbed gold–sulfur binding prevails in self-assembled monolayers." *Nature chemistry* **11**, 351-358 (2019).
9. Kamenetska, M., Su Ying Quek, A. C. Whalley, M. L. Steigerwald, H. J. Choi, Steven G. Louie, C. Nuckolls, M. S. Hybertsen, J. B. Neaton, and L. Venkataraman. "Conductance and geometry of pyridine-linked single-molecule junctions." *Journal of the American Chemical Society* **132**, 6817-6821 (2010).
10. Yu, Hao, Songsong Li, Kenneth E. Schwieter, Yun Liu, Boran Sun, Jeffrey S. Moore, and Charles M. Schroeder. "Charge transport in sequence-defined conjugated oligomers." *Journal of the American Chemical Society* **142**, 4852-4861 (2020).
11. Cheng, Z-L., Rachid Skouta, Hector Vazquez, Jonathan R. Widawsky, Severin Schneebeli, W. Chen, Mark S. Hybertsen, Ronald Breslow, and Latha Venkataraman. "In situ formation of highly conducting covalent Au–C contacts for single-molecule junctions." *Nature nanotechnology* **6**, 353-357 (2011).
12. Starr, Rachel L., Tianren Fu, Evan A. Doud, Ilana Stone, Xavier Roy, and Latha Venkataraman. "Gold–carbon contacts from oxidative addition of aryl iodides." *Journal of the American Chemical Society* **142**, 7128-7133 (2020).

13. Bejarano, Francesc, Ignacio Jose Olavarria-Contreras, Andrea Droghetti, Ivan Rungger, Alexander Rudnev, Diego Gutiérrez, Marta Mas-Torrent et al. "Robust organic radical molecular junctions using acetylene terminated groups for C–Au bond formation." *Journal of the American Chemical Society* **140**, 1691-1696 (2018).
14. Pla-Vilanova, Pepita, Albert C. Aragonès, Simone Ciampi, Fausto Sanz, Nadim Darwish, and Ismael Diez-Perez. "The spontaneous formation of single-molecule junctions via terminal alkynes." *Nanotechnology* **26**, 381001 (2015).
15. Peiris, Chandramalika R., Yan B. Vogel, Anton P. Le Brun, Albert C. Aragonès, Michelle L. Coote, Ismael Díez-Pérez, Simone Ciampi, and Nadim Darwish. "Metal–single-molecule–semiconductor junctions formed by a radical reaction bridging gold and silicon electrodes." *Journal of the American Chemical Society* **141**, 14788-14797 (2019).
16. Hines, Thomas, Ismael Díez-Pérez, Hisao Nakamura, Tomomi Shimazaki, Yoshihiro Asai, and Nongjian Tao. "Controlling formation of single-molecule junctions by electrochemical reduction of diazonium terminal groups." *Journal of the American Chemical Society* **135**, 3319-3322 (2013).
17. Huang, Xiaoyan, Chun Tang, Jieqiong Li, Li-Chuan Chen, Jueting Zheng, Pei Zhang, Jiabo Le et al. "Electric field–induced selective catalysis of single-molecule reaction." *Science Advances* **5**, eaaw3072 (2019).
18. Lin, Junfeng, Yaxin Lv, Kai Song, Xuwei Song, Hongjun Zang, Pingwu Du, Yaping Zang, and Daoben Zhu. "Cleavage of non-polar C (sp 2)–C (sp 2) bonds in cycloparaphenylenes via electric field-catalyzed electrophilic aromatic substitution." *Nature Communications* **14**, 293 (2023).
19. Martín, Santiago, Iain Grace, Martin R. Bryce, Changsheng Wang, Rukkiat Jitchati, Andrei S. Batsanov, Simon J. Higgins, Colin J. Lambert, and Richard J. Nichols. "Identifying diversity in nanoscale electrical break junctions." *Journal of the American Chemical Society* **132**, 9157-9164 (2010).
20. Frisenda, Riccardo, Vera AEC Janssen, Ferdinand C. Grozema, Herre SJ Van Der Zant, and Nicolas Renaud. "Mechanically controlled quantum interference in individual π-stacked dimers." *Nature chemistry* **8**, 1099-1104 (2016).
21. Wei, Yujing, Liang Li, Julia E. Greenwald, and Latha Venkataraman. "Voltage-modulated van der Waals interaction in single-molecule junctions." *Nano Letters* **23**, 567-572 (2023).
22. Yu, Hao, Jialing Li, Songsong Li, Yun Liu, Nicholas E. Jackson, Jeffrey S. Moore, and Charles M. Schroeder. "Efficient intermolecular charge transport in π-stacked pyridinium dimers using cucurbit [8] uril supramolecular complexes." *Journal of the American Chemical Society* **144**, 3162-3173 (2022).
23. Coropceanu, Veaceslav, Jérôme Cornil, Demetrio A. da Silva Filho, Yoann Olivier, Robert Silbey, and Jean-Luc Brédas. "Charge transport in organic semiconductors." *Chemical reviews* **107**, 926-952 (2007).
24. Yi, Yuanping, Veaceslav Coropceanu, and Jean-Luc Brédas. "A comparative theoretical study of exciton-dissociation and charge-recombination processes in

oligothiophene/fullerene and oligothiophene/perylenediimide complexes for organic solar cells." *Journal of Materials Chemistry* **21**, 1479-1486 (2011).
25. Solomon, Gemma C., Carmen Herrmann, Josh Vura-Weis, Michael R. Wasielewski, and Mark A. Ratner. "The chameleonic nature of electron transport through π-stacked systems." *Journal of the American Chemical Society* **132**, 7887-7889 (2010).
26. Delgado, M. Carmen Ruiz, Eung-Gun Kim, Demétrio A. da Silva Filho, and Jean-Luc Bredas. "Tuning the charge-transport parameters of perylene diimide single crystals via end and/or core functionalization: a density functional theory investigation." *Journal of the American Chemical Society* **132**, 3375-3387 (2010).
27. Pan, Xiaoyun, Enrique Montes, Wudmir Y. Rojas, Brent Lawson, Héctor Vázquez, and Maria Kamenetska. "Cooperative Self-Assembly of Dimer Junctions Driven by π Stacking Leads to Conductance Enhancement." *Nano Letters* **23**, 6937-6943 (2023).
28. Tang, Yongxiang, Yu Zhou, Dahai Zhou, Yaorong Chen, Zongyuan Xiao, Jia Shi, Junyang Liu, and Wenjing Hong. "Electric field-induced assembly in single-stacking terphenyl junctions." *Journal of the American Chemical Society* **142**, 19101-19109 (2020).
29. Wang, Wesley, Nicholas H. Angello, Daniel J. Blair, Theodore Tyrikos-Ergas, William H. Krueger, Kameron NS Medine, Antonio J. LaPorte, Joshua M. Berger, and Martin D. Burke. "Rapid automated iterative small-molecule synthesis." *Nature Synthesis*, 1-8 (2024).
30. Li, Songsong, Hao Yu, Kenneth Schwieter, Kejia Chen, Bo Li, Yun Liu, Jeffrey S. Moore, and Charles M. Schroeder. "Charge transport and quantum interference effects in oxazole-terminated conjugated oligomers." *Journal of the American Chemical Society* **141**, 16079-16084 (2019).
31. Li, Bo, Hao Yu, Elena C. Montoto, Yun Liu, Songsong Li, Kenneth Schwieter, Joaquín Rodríguez-López, Jeffrey S. Moore, and Charles M. Schroeder. "Intrachain charge transport through conjugated donor–acceptor oligomers." *ACS Applied Electronic Materials* **1**, 7-12 (2018).
32. Ciampi, Simone, Nadim Darwish, Heather M. Aitken, Ismael Díez-Pérez, and Michelle L. Coote. "Harnessing electrostatic catalysis in single molecule, electrochemical and chemical systems: a rapidly growing experimental tool box." *Chemical Society Reviews* **47**, 5146-5164 (2018).
33. Li, Songsong, Edward R. Jira, Nicholas H. Angello, Jialing Li, Hao Yu, Jeffrey S. Moore, Ying Diao, Martin D. Burke, and Charles M. Schroeder. "Using automated synthesis to understand the role of side chains on molecular charge transport." *Nature communications* **13**, 2102 (2022).
34. Gillis, Eric P., and Martin D. Burke. "A simple and modular strategy for small molecule synthesis: iterative Suzuki− Miyaura coupling of B-protected haloboronic acid building blocks." *Journal of the American Chemical Society* **129**, 6716-6717 (2007).
35. Ryan, Seán TJ, Ryan M. Young, James J. Henkelis, Nema Hafezi, Nicolaas A. Vermeulen, Andreas Hennig, Edward J. Dale et al. "Energy and electron transfer dynamics within a series of perylene diimide/cyclophane systems." *Journal of the American Chemical Society* **137**, 15299-15307 (2015).

36. Angello, Nicholas H., David M. Friday, Changhyun Hwang, Seungjoo Yi, Austin H. Cheng, Tiara C. Torres-Flores, Edward R. Jira et al. "Closed-loop transfer enables artificial intelligence to yield chemical knowledge." *Nature* (2024), 1-8.
37. Wakamatsu, Satoshi, Uichi Akiba, and Masamichi Fujihira. "Electronic tunneling through a single molecule embedded in self-assembled monolayer matrices." *Colloids and Surfaces A: Physicochemical and Engineering Aspects* **198**, 785-790 (2002).
38. Duan, Lili, and Simon J. Garrett. "An investigation of rigid p-methylterphenyl thiol self-assembled monolayers on Au (111) using reflection− absorption infrared spectroscopy and scanning tunneling microscopy." *The Journal of Physical Chemistry B* **105**, 9812-9816 (2001).
39. Heimel, Georg, Dieter Somitsch, Peter Knoll, and Egbert Zojer. "Ab initio study of vibrational anharmonic coupling effects in oligo (para-phenylenes)." *The Journal of chemical physics* **116**, 10921-10931 (2002).
40. Maya, F., & Tour, J. M. Synthesis of terphenyl oligomers as molecular electronic device candidates. *Tetrahedron* **60**, 81-92 (2004).
41. Feng, Anni, Yu Zhou, Mohammed AY Al-Shebami, Lichuan Chen, Zhichao Pan, Wei Xu, Shiqiang Zhao et al. "σ–σ Stacked supramolecular junctions." *Nature Chemistry* **14**, 1158-1164 (2022).
42. Samajdar, Rajarshi, Moeen Meigooni, Hao Yang, Jialing Li, Xiaolin Liu, Nicholas E. Jackson, Martín A. Mosquera, Emad Tajkhorshid, and Charles M. Schroeder. "Secondary structure determines electron transport in peptides." *Proceedings of the National Academy of Sciences* **121**, e2403324121 (2024).
43. Liu, Xiaolin, Hao Yang, Hassan Harb, Rajarshi Samajdar, Toby J. Woods, Oliver Lin, Qian Chen et al. "Shape-persistent ladder molecules exhibit nanogap-independent conductance in single-molecule junctions." *Nature Chemistry*, 1-9 (2024).
44. Adak, Olgun, Ethan Rosenthal, Jeffery Meisner, Erick F. Andrade, Abhay N. Pasupathy, Colin Nuckolls, Mark S. Hybertsen, and Latha Venkataraman. "Flicker noise as a probe of electronic interaction at metal–single molecule interfaces." *Nano letters* **15**, 4143-4149 (2015).
45. Fu, Tianren, Shanelle Smith, María Camarasa-Gómez, Xiaofang Yu, Jiayi Xue, Colin Nuckolls, Ferdinand Evers, Latha Venkataraman, and Sujun Wei. "Enhanced coupling through π-stacking in imidazole-based molecular junctions." *Chemical Science* **10**, 9998-10002 (2019).
46. Adak, Olgun, Ethan Rosenthal, Jeffery Meisner, Erick F. Andrade, Abhay N. Pasupathy, Colin Nuckolls, Mark S. Hybertsen, and Latha Venkataraman. "Flicker noise as a probe of electronic interaction at metal–single molecule interfaces." *Nano letters* **15**, 4143-4149 (2015).
47. Tan, Ying, Jialing Li, Songsong Li, Hao Yang, Teng Chi, Stephen B. Shiring, Kangying Liu, Brett M. Savoie, Bryan W. Boudouris, and Charles M. Schroeder. "Enhanced electron transport in nonconjugated radical oligomers occurs by tunneling." *Nano letters* **23**, 5951-5958 (2023).
48. Bard, Allen J., and Larry R. Faulkner. "Fundamentals and Applications, New York: Wiley, 2001." 1364-1365 (2002).

49. Li, Jialing, Sanja Pudar, Hao Yu, Songsong Li, Jeffrey S. Moore, Joaquín Rodríguez-López, Nicholas E. Jackson, and Charles M. Schroeder. "Reversible switching of molecular conductance in viologens is controlled by the electrochemical environment." *The Journal of Physical Chemistry C* **125**, 21862-21872 (2021).
50. Kumar, Shankar, et al. "The weighted histogram analysis method for free-energy calculations on biomolecules. I. The method." *Journal of computational chemistry* **13**, 1011-1021 (1992).

Acknowledgements

This work was supported by the U.S. Department of Energy, Office of Science, Basic Energy Sciences under Award No. DE-SC0022035 for H.Y., X.L., M.M., J.S.M., E.T., and C.M.S., the National Science Foundation under Award 2227399 and the Army Research Office under Cooperative Agreement Number W911NF-22-2-0246 for R.S. and C.M.S. The views and conclusions contained in this document are those of the authors and should not be interpreted as representing the official policies, either expressed or implied, of the Army Research Office or the U.S. Government. The U.S. Government is authorized to reproduce and distribute reprints for Government purposes notwithstanding any copyright notation herein. This work was supported by the Molecule Maker Lab Institute, an AI Research Institutes program supported by the US National Science Foundation under grant no. 2019897 for S.Y. We gratefully acknowledge Furong Sun and the UIUC Mass Spectrometry Lab. S.P. is grateful for support from the National Science Foundation Graduate Research Fellowship. M.P. is grateful for the support of Beckman Institute for Advanced Science and Technology Graduate Fellows Program with support from the Arnold and Mabel Beckman Foundation.

Author contributions

R.S., H.Y., S.Y., and C.M.S. conceived this study. R.S. and H.Y. performed STM-BJ experiments, data analysis, and unsupervised machine learning. S.Y. performed chemical synthesis and characterization. C.W performed MD simulations. M.P. and S.P. carried out bulk scale electrochemistry, electrolysis, and spectroscopy experiments. R.S. performed the NEGF-DFT calculations. M.M., X.L., J.R. assisted in experiments and simulations. The manuscript was written by R.S., H.Y. and C.M.S. with contribution from all authors.

Competing Interests

The authors declare no competing interests.

Additional Information

Supplementary information contains supplementary figures, supplementary tables, and supplementary text.